Spatial-seasonal patterns reveal large-scale atmospheric controls on Asian Monsoon precipitation water isotope ratios Zhongyin Cai^{a,b,f*}, Lide Tian^{a,c,d,e*}, Gabriel J Bowen^b ^a Key Laboratory of Tibetan Environment Changes and Land Surface Processes, Institute of Tibetan Plateau Research, Chinese Academy of Sciences, Beijing 100101, China ^b Department of Geology and Geophysics, University of Utah, Salt Lake City, Utah 84112, USA ^c Institute of International Rivers and Eco-security, Yunnan University, Kunming, Yunnan 650091, China ^d CAS Center for Excellence in Tibetan Plateau Earth Sciences, Beijing 100101, China ^e College of Resource and Environment, University of Chinese Academy of Sciences, Beijing, 100190, China ^f University of Chinese Academy of Sciences, Beijing 100049, China *Corresponding authors: Lide Tian (ldt@itpcas.ac.cn); Zhongyin Cai (czypil@gmail.com)

Abstract:

21

22

23

24

25

26

27

28

29

30

31

32

33

34

35

36

37

38

39

40

41

Correlated seasonal variation in precipitation amount and its oxygen isotope ratios (δ^{18} O) has long been observed and frequently invoked in the interpretation of paleo-δ¹⁸O records from the Asian Monsoon (AM) region. However, the underlying cause of the observed seasonal δ^{18} O variation is still under debate. Precipitation δ^{18} O values show a single, consistent seasonal pattern across the region, with high values in pre-monsoon (late-spring to early-summer) and low values in the monsoon mature (midto late-summer) periods. We tested three hypotheses that may give rise to the measured precipitation δ^{18} O pattern, involving variation in: 1) local precipitation, 2) moisture sources, and 3) convection in moisture source regions. We show that seasonal precipitation amounts across the AM region exhibit two pattern types: pre-monsoon peak or monsoon mature peak, and thus do not provide a consistent explanation for the isotopic pattern. We test the hypotheses that changing moisture sources or moisture source isotope ratios drive the seasonal isotopic pattern using a combination of Lagrangian moisture source attribution and output from an isotope-enabled General Circulation Model (LMDZ4), but find little seasonal variation in moisture sources; that which does exist is not consistent with the observed isotopic change. Instead, we show that the precipitation δ^{18} O transition from pre-monsoon to monsoon mature stage is correlated with intensification of convective activity in moisture source regions, which is the result of monsoon establishment and northward migration of the Intertropical Convergence Zone (ITCZ). We propose that light water vapor, transferred to the lower-troposphere through downdrafts and evaporation of rain in the vicinity of intense convection, is advected to the AM region and labels precipitation during the monsoon mature period. These results demonstrate that precipitation δ^{18} O in the AM region more strongly reflect large-scale atmospheric dynamics than local precipitation amount or

- 42 moisture source, guiding the interpretation of paleo-isotope data from this region.
- **Keywords:** Oxygen isotope; precipitation; seasonal variation; moisture source; convection; Asian
- 44 Monsoon

1 Introduction

Monsoon regions are characterized by strong seasonal reversal in atmospheric circulation and associated wet/dry alternation. The Asian Monsoon (AM) is the archetypal monsoon system (Wang, 2006). In the region it affects human wellbeing, which is intimately linked to water resources, natural disasters such as heavy rainfalls and droughts, and other weather phenomena. Thus, understanding the dynamics and variability of the AM is of great scientific and socioeconomic importance.

Precipitation isotope signals (δD and $\delta^{18}O$, both in modern precipitation and reconstructed from proxy archives), which vary in response to climatic system processes (e.g., Araguás-Araguás et al., 1998; Bowen and Wilkinson, 2002; Dansgaard, 1964; Rozanski et al., 1993), have proven valuable in understanding present monsoon climate and providing opportunities to study the history of the monsoon as far back as 640,000 years ago (e.g., Cheng et al., 2016; Thompson et al., 2000; Wang et al., 2001; Yao et al., 2013). The "amount effect" (the inverse correlation between monthly precipitation $\delta^{18}O$ and precipitation amount) (Dansgaard, 1964) is a prominent empirical relationship derived from modern isotopic studies in tropical and monsoon regions. The amount effect has been documented and studied in the AM region, where it can be observed as anti-phase seasonal variations in precipitation amount and precipitation $\delta^{18}O$ values at some (e.g., Araguás-Araguás et al., 1998; Yao et al., 2013), but not all sites (e.g., Breitenbach et al., 2010; Tang et al., 2015), and has been adopted in the interpretation of many paleoclimate records in the region (e.g., Tan et al., 2018; Tian et al., 2003).

There is now a strong consensus that the empirical amount effect is not mechanistically associated with variation in local precipitation amount, but rather reflects large-scale atmospheric phenomena. Researchers studying the AM region have explored three different types of explanations for the amount effect observed in this region. First, some work has continued to focus on the traditional association of precipitation δ^{18} O with local precipitation amount, which presumably reflects the extent of rainout and associated isotopic fractionation in different systems. This negative relationship has remained of particular interest in paleoclimate studies, where researchers seek to reconstruct local precipitation at sites where proxy records were obtained (e.g., Dayem et al., 2010; Tan et al., 2018).

Second, as early as 1989, scientists found a sharp decrease in snowfall δ^{18} O values on the Tibetan Plateau during the monsoon onset (from late May to early June) and attributed this transition to changes in moisture sources, with high values associated with continental moisture and low values with oceanic moisture (Yao et al., 1991). A later regional study also attributed seasonal variation in AM precipitation δ^{18} O to seasonally changing moisture sources (Araguás-Araguás et al., 1998), and this moisture source hypothesis has been widely advanced to explain precipitation isotope patterns in the AM region (e.g., Breitenbach et al., 2010; Peng et al., 2010; Tang et al., 2015; Xie et al., 2011). Robust support for and mechanistic understanding of this hypothesis remains elusive, however, and it is not clear whether there is actually a large shift in moisture sources during the monsoon season or whether varying vapor source δ^{18} O values can explain the precipitation isotope observations. A recent moisture source study in the East AM region, for example, showed that despite strong westerly water vapor transport in winter the majority of moisture contributing to precipitation came from the tropical oceans (Li et al., 2016).

A third set of hypotheses for the AM amount effect focuses on upstream atmospheric processes,

such as convective intensity and moisture convergence. Convective processes have the potential to alter local precipitation and vapor isotope compositions in the source regions (Kurita, 2013; Lee et al., 2007; Moore et al., 2014; Risi et al., 2008a; Worden et al., 2007), and the propagation of this vapor to downstream sites could influence precipitation isotope ratios in the AM region (Cai and Tian, 2016a; He et al., 2015; Tang et al., 2015). These processes have been shown to affect precipitation isotope ratios at short timescales (event to interannual scales) in the AM region (e.g., Cai et al., 2017; Tang et al., 2015) and other monsoon regions (e.g., Risi et al., 2008b; Vimeux et al., 2005). For instance, Tang et al. (2015) suggested that the combined effects of source region location and upstream rainout cause intra-seasonal precipitation δ^{18} O variation at Nanjing during the summer monsoon. Cai and Tian (2016a) suggested that seasonal variation in East AM precipitation δ^{18} O values is related to cloud-top height variation associated with monsoon convective intensity, raising questions about the significance of moisture source as a control on regional precipitation isotope ratios.

These uncertainties in our understanding of modern precipitation $\delta^{18}O$ variations (the amount effect and controlling mechanisms), in part, hinder the interpretation of paleo- $\delta^{18}O$ records from natural archives, such as ice cores from the Tibetan Plateau (e.g., Thompson et al., 2000), speleothems from southeast China (e.g., Liu et al., 2015), and tree ring cellulose (e.g., Xu et al., 2015). For example, whether speleothem $\delta^{18}O$ records from southeast China are robust proxies for East AM precipitation amount or not remains an open discussion (e.g., Dayem et al., 2010; Liu et al., 2015; Tan et al., 2018). As new paleo- $\delta^{18}O$ records are developed at a growing rate and new technology allows resolution of sub-annual paleo- $\delta^{18}O$ records in this region (e.g., Xu et al., 2015), a clearer understanding of modern precipitation $\delta^{18}O$ variation is becoming more important and urgent.

Here we spatially characterize seasonal variations in precipitation amount and precipitation δ^{18} O from station data and gridded data products to examine the amount effect across the AM region. Based on the results we identify two distinct seasonal precipitation patterns in the region, one dominant in areas of southeast China where precipitation peaks before the summer monsoon onset, and one characteristic of much of the rest of the region with maximum precipitation during the mature stage of the summer monsoon. Focusing on the region dominated by the pre-monsoon maximum, we conduct daily back trajectory calculation over ten years to determine moisture sources during these two seasons and infer moisture source isotopic composition using an isotope-enabled General Circulation Model (LMDZ4). To test whether results from this sub-region are applicable to the broader AM region, we conduct a comparative study on a sub-region of the monsoon mature domain in south Asia. Our results suggest that moisture source variation does not offer a consistent explanation for precipitation isotope variation within both monsoon sub-regions, and we propose instead that this variation is driven by upstream convective processes that isotopically deplete lower-troposphere vapor within vapor source regions. Seasonal variation in precipitation δ^{18} O is thus controlled largely by source region convection and associated large-scale atmospheric circulation.

2 Data and methods

105

106

107

108

109

110

111

112

113

114

115

116

117

118

119

120

121

122

123

124

125

2.1 Isotope and climate data

Our work uses precipitation δ^{18} O observations from several sources to obtain data from across the AM region. These data include event-based precipitation δ^{18} O data at Lhasa, southern Tibetan Plateau from 1993-2014 (Cai et al., 2017) and at Lulang, southeast Tibetan Plateau from 2007-2014 (Yang et al., 2017); event-based precipitation δ^{18} O data at Guangzhou, southeast China from 2007-2009 (Xie et al.,

2011); and monthly precipitation δ^{18} O from Global Network of Isotopes in Precipitation (GNIP) stations in the AM region (https://nucleus.iaea.org/wiser). Associated precipitation amount data from the isotope monitoring stations are also used in this work. For the event-based data, we calculated precipitationamount weighted monthly mean δ^{18} O values. GNIP data are also available for the Lhasa and Guangzhou stations, but with different temporal coverage from the event-based data. In these cases both data sources were combined to achieve longer temporal coverage. Many GNIP stations have temporal gaps in their records. Here we used only those stations with adequate data to estimate long-term monthly mean values for all 12 months (section 3). In most cases, these long-term monthly mean values represent multi-year average, with a few exceptions in winter months due to sparse precipitation. We note that some of these stations only have data coverage of several years. However, temporal variability of precipitation δ^{18} O at annual and longer timescales is much smaller than seasonal variability. Therefore, we argue that the temporally short data coverage at these stations will only have a small impact on the estimated seasonal δ¹⁸O variability. One station, Sylhet, was excluded from the analyses in section 3 given that data for December were not available, but provided an adequate monthly record to be used in section 4.4.

126

127

128

129

130

131

132

133

134

135

136

137

138

139

140

141

142

143

144

145

146

In order to classify different modes of variability across the AM region we conducted cluster analysis on the long-term mean monthly precipitation amount records from the observational stations. We used the Hierarchical Cluster Analysis tool provided by the OriginPro software package. Before clustering, we normalized long-term mean monthly values (precipitation amount and δ^{18} O, respectively) using the equation: $z = (x - \mu)/\sigma$, where: z is the normalized long-term mean monthly value (z-score), z represents the observed long-term mean monthly value, z is the annual mean value, and z is the standard deviation of the 12 long-term mean monthly values at each station.

To compare seasonal precipitation patterns between stations and regions we defined a seasonal index. Given that the onset of the summer monsoon over most of south-east Asia is during late-May to June (Wang and LinHo, 2002), we use data from April-May to represent the pre-monsoon season and July-August the monsoon season. The seasonal index is defined as: $x_{SI} = (x_{am} - x_{ja})/\sigma$, where: x is average precipitation amount or δ^{18} O and subscript am or ja represents April-May or July-August, respectively.

In order to evaluate precipitation patterns across the AM region we used Version 7 of the Tropical Rainfall Measuring Mission (TRMM) Multi-Satellite Precipitation Analysis (3B43) with a $0.25^{\circ} \times 0.25^{\circ}$ resolution from 1998-2016 (Huffman et al., 2007). For precipitation δ^{18} O, we used the gridded data products from the IsoMAP platform (Bowen et al., 2017) created at $0.5^{\circ} \times 0.5^{\circ}$ resolution over the continents. IsoMAP applies combined nonlinear regression and geostatistical modeling methods to predict precipitation δ^{18} O between data stations (Bowen, 2008; Bowen and Wilkinson, 2002). Independent variables in the models used here included latitude, latitude squared, and altitude, which are known to be related to precipitation isotope ratios globally (Bowen and Wilkinson, 2002), as well as longitude and the square of longitude, which serve as a proxy for continentality effects expressed in precipitation δ^{18} O values in the AM region (Aggarwal et al., 2004; Cai and Tian, 2016b).

To investigate how the precipitation $\delta^{18}O$ is linked with upstream processes, we analyzed satellite vapor isotopologue (HDO and H₂O) retrievals from Tropospheric Emission Spectrometer (TES) during 2006-2010. We used the recent version 6 TES Lite product, which offers improved sensitivity across a wider altitude range (925-350 hPa) than previous versions of the TES data products (Worden et al., 2006; Worden et al., 2012). We only used the data for which the available degrees of freedom for signals

exceeded 0.5 and species retrieval quality was classified as "1" to assure data quality. Individual TES δD measurements typically have a precision of about 10-15%, but when averaged over large spatial domains the precision can be improved to 1-2% (Risi et al., 2012; Worden et al., 2006). Although vapor δD was used in this study, we note that δD and $\delta^{18}O$ values of meteoric waters usually vary in parallel (e.g., Dansgaard, 1964; Rozanski et al., 1993).

We used cloud-top pressure and temperature (CTP and CTT) data from the International Satellite Cloud Climatology Project (ISCCP) D2 dataset, with a spatial resolution of 280 km \times 280 km and coverage from 1984-2009 (Rossow and Schiffer, 1999), as indicators of convective intensity. ERA-Interim data from the European Centre for Medium-Range Weather Forecasts (ECWMF, 1979-2016) at 37 pressure levels and a resolution of $1^{\circ} \times 1^{\circ}$ (Dee et al., 2011) were used in back trajectory calculations (see below) and to characterize total column moisture flux, moisture convergence/divergence, and atmospheric circulation. Vertical velocity at 500 hPa (ω), which measures the strength of vertical motion in the mid-troposphere, was used to estimate the mean latitude of the center of Intertropical Convergence Zone (ITCZ). More specifically, the mean positon of ITCZ was calculated as the weighted (by the absolute value of ω) mean latitude of ERA grid cells with ascending air (ω <0).

2.2 Back trajectory calculation and moisture source diagnostic

Air mass back trajectories, initiated four times daily (at UTC 00:00, 06:00, 12:00, and 18:00) and moved backward with winds for 240 hours (10 days), were computed at 6 hour intervals from the Hybrid Single-Particle Lagrangian Integrated Trajectory (HYSPLIT) model (Stein et al., 2015). The air parcels were released at 1500 m above ground level (AGL), a level with strong horizontal moisture transport that approximates the expected condensation level in this region (e.g., Aggarwal et al., 2004;

Breitenbach et al., 2010).

Changes in specific humidity (q) have previously been used to diagnose moisture sources in a Lagrangian framework as they reflect precipitation and evaporation along the trajectory (e.g., Li et al., 2016; Sodemann et al., 2008). We adopted this concept to estimate moisture source locations along our back trajectories, and their contribution to precipitating back trajectories initiated from the AM region. We used two criteria to identify precipitating trajectories: 1) initial relative humidity (at t = 0) more than 80%; 2) specific humidity change at first time interval ($\Delta q_0 = q_{t=-6} - q_{t=0}$) more than 0.2 g/kg ($\Delta q_0 > 0.2 \, g / kg$). The relative humidity threshold identifies periods when clouds and precipitation are likely to exist in the ECMWF model. The specific humidity decrease at the first time interval is assumed to reflect precipitation at the starting point, and the minimum specific humidity change threshold helps avoid spurious identification of moisture sinks or uptakes (Sodemann et al., 2008).

For precipitating trajectories, periods of specific humidity increase (forward in time) were identified as moisture uptake periods and we recorded the average location during each uptake interval as a single source location for that trajectory. Each trajectory may contain several moisture uptake events. However, air masses may also experience precipitation (specific humidity decrease) during periods prior to *t*=0, thus reducing the contribution of earlier uptake events to precipitation at the back trajectory staring point. Moisture lost from the air mass was subtracted from the mass of water carried forward from the preceding uptake event(s). The remaining moisture uptake amounts were used to calculate the relative contribution of each moisture source to precipitation delivered by a given trajectory and map the spatial location of moisture sources contributing to AM precipitation across all trajectories. Further, to isolate uptake associated with surface evaporation, we divided moisture uptake at each source

location into two parts: uptake within the planetary boundary layer (linked with surface evaporation) and in the free troposphere (above planetary boundary layer; linked with processes other than surface evaporation, such as convective moistening). In the HYSPLIT model, the planetary boundary layer was derived from the temperature profile. As in Sodemann et al. (2008), we scaled the estimated boundary layer height by a factor of 1.5 to account for small-scale variability and model underestimation of marine boundary layer heights. A more detailed mathematic description of the moisture source identification and attribution method is given in Sodemann et al. (2008). We conducted this analysis for a ten-year period (2000-2009) for April, May, July, and August. We did not find any significant difference between results from the first half (2000-2005) and the whole analysis period (2000-2009), which suggests that our results are stable and reflective of climatological normals.

To assess potential differences in the isotopic composition of moisture sources from different locations and times we used output (evaporation flux of the H_2O , HDO, and $H_2^{18}O$ isotopologues) from the LMDZ4 isotope-enabled General Circulation Model, available from the Stable Water Isotope Intercomparison Group, Phase 2 (SWING2) project (Risi et al., 2012). LMDZ4 has a $2.5^{\circ} \times 3.75^{\circ}$ horizontal resolution and 19 vertical levels. Land surface evapotranspiration at each grid cell is calculated as a single unfractionated flux. Kinetic effects during sea surface evaporation are represented. We used output from the nudged version, which is forced by Atmospheric Model Intercomparison Project (AMIP2) sea surface temperatures and nudged by ECMWF re-analyses wind fields at each level to constrain model simulations toward actual meteorology (Risi et al., 2010; Risi et al., 2012).

3 Results

Cluster analysis on normalized long-term mean monthly precipitation amount values suggests that

stations across the AM region can be divided into five groups (Fig. 1; Fig. S1). The first group is characterized by high rainfall amount during late-spring to early-summer, but relatively less rainfall during the summer monsoon season (Fig. 1a). These stations are located in southeast China (Fig. 2a). Groups 2-4 are distributed across much of the rest of the AM region and are all characterized by peak rainfall during the summer monsoon season, with differences in the timing and pace of the onset/end of monsoon precipitation among groups (Fig. 1b-1d and 2a). A single station on the southeast coast of China (Fig. 2a), Fuzhou, shows a distinct pattern with double peaks during late-spring to early-summer and September (Fig. 1e) and clusters away from the other stations (group 5).

In contrast, precipitation $\delta^{18}O$ values show consistent seasonal variation across these groups, with high values before the onset of summer monsoon and low values during the monsoon season (Fig. 1f-1j). Precipitation $\delta^{18}O$ values rebound at most sites after the withdrawing of the summer monsoon (Fig. 1f-1j). A few local exceptions exist, where low $\delta^{18}O$ values persist during the post-monsoon season, which are related to cyclonic activity (Lekshmy et al., 2015).

The spatial distribution of precipitation seasonal index values derived from station and gridded data are consistent, and support a spatially coherent, bimodal pattern of precipitation seasonality across the AM region. Pre-monsoon maximum precipitation is characteristic of southeast China, with the monsoon mature pattern dominating elsewhere (Fig. 2a and 2b). Gridded IsoMAP precipitation isotope data also support the station observations, indicating that across the region precipitation δ^{18} O is high during April-May but low during July-August across the AM region (Fig. 2c). For most of the AM region, the precipitation δ^{18} O difference between these two periods is higher than 1.5 standard deviations of the long-term mean monthly values throughout the year. Thus, the precipitation δ^{18} O during April-May and

July-August represents the two opposite extremes in terms of annual variation.

4 Discussion

252

253

254

255

256

257

258

259

260

261

262

263

264

265

266

267

268

269

270

271

272

To investigate the controlling mechanisms of seasonal precipitation $\delta^{18}O$ variation, we test the aforementioned (section 1) three hypotheses: local precipitation, continental-oceanic moisture source shift, and convection in moisture source regions, in the following sections. Finally, a brief discussion on paleoclimate implications and limitations is given.

4.1 Local precipitation amount

The spatially varying seasonal pattern in precipitation coupled with the consistent seasonal pattern in precipitation δ^{18} O values across the AM region implies a decoupling of δ^{18} O from local precipitation. Correlation analysis between IsoMAP derived precipitation δ^{18} O and local precipitation amount shows that the traditionally-recognized amount effect can be identified in Indochina and northeast India but is insignificant in southeast China (Fig. 2d). In general, the results from gridded IsoMAP data are consistent with station observations. However, stations in northeast India are very sparse and correlations between precipitation δ^{18} O and precipitation amount at the two sites in Bangladesh are insignificant (Fig. 2d). Analysis of the relationship between monthly precipitation δ^{18} O and precipitation amount for three stations in southeast China shows that precipitation amounts explain less than 13% of the δ^{18} O variability (Fig. 3). These results do not support the use of precipitation δ^{18} O values in southeast China as a proxy for precipitation amount, and instead suggest that large-scale dynamical controls more likely govern precipitation isotope ratios across the AM region. In order to further evaluate the mechanisms controlling precipitation isotope ratios and compare between pre-monsoon and monsoon mature regions we defined two focus areas, R East (108-120°E, 24-30°N; Fig. 2a) representing the pre-monsoon (section 4.2 and

4.3) and R_STP (83-95°E, 21-27°N) representing monsoon mature (section 4.4), for analysis.

4.2 Moisture sources

273

274

275

276

277

278

279

280

281

282

283

284

285

286

287

288

289

290

291

292

293

The second paradigm invoked to explain seasonal AM precipitation δ^{18} O variation is continentaloceanic moisture source shift (e.g., Araguás-Araguás et al., 1998; Peng et al., 2010; Tang et al., 2015; Xie et al., 2011; Yao et al., 1991; Yao et al., 2013). Some support for this idea has come from previous air mass back trajectory studies (e.g., Xie et al., 2011), but these analyses have not considered moisture content along trajectories. The resulting analyses dominantly reflect wind fields and may be misleading because moisture contributions to precipitation may not scale directly with the dominant wind fields (Li et al., 2016). We test this idea using a combination of a Lagrangian moisture source diagnostic method (Li et al., 2016; Sodemann et al., 2008) and analysis of evaporation isotopologue fluxes from a General Circulation Model (Risi et al., 2012). To estimate moisture sources of R East precipitation, we divided R East into grid cells with 3° × 3° resolution and air parcels were released at the center of each grid cell (Fig. 4). Moisture sources were aggregated on a monthly basis. Comparison between monthly total attributed moisture amount (sum of projected moisture amounts at all uptake intervals) and regional mean TRMM precipitation amount shows significant correlations (r = 0.72, p<0.01) (Fig. S2). This relationship suggests that the method used here to diagnose R East precipitation sources accurately reflects precipitation variability.

The spatial distribution of moisture source contributions to April-May precipitation in R_East shows that moisture mainly originates from the northern South China Sea (Fig. 4a). This result is in qualitative agreement with the general circulation patterns reflected in the moisture flux field and moisture flux divergence (Fig. S3a). During this period, the summer monsoon has not yet commenced

and water vapor originates mainly from the sea surface on the flank of the western Pacific subtropical high (WPSH). The convergence of the southern branch of the westerlies and the southwest flow at the flank of the WPSH with cold air from the north forms a regional vapor convergence zone driving premonsoon precipitation across R_East (Fig. S3a). In addition, spatial patterns of moisture sources from surface evaporation (within boundary layer; Fig. 4c) are similar to the spatial patterns of combined moisture source (including the boundary layer and free troposphere; Fig. 4a). Overall, moisture uptake within the boundary layer accounts for 71% of the total moisture contribution, and marine boundary layer moisture contributions are the dominant source during this period, comprising 72% of the boundary layer uptake based on our attribution analysis.

Moisture sources for July-August precipitation in R_East are shifted southwest relative to the premonsoon period (Fig. 4b) due to the influence of summer monsoon flow (Fig. S3b). Most moisture uptake happens in the northwestern South China Sea and nearby continental regions. Although a substantial number of back trajectories trace back to the Indian Ocean, the moisture contribution from that basin is limited due to strong downstream convergence and precipitation over land regions east of the Bay of Bengal (Fig. S3b). The moisture uptake within the boundary layer (Fig. 4c) is 67% (relative to total moisture uptake), and marine boundary layer moisture contribution is 73% of that amount during July-August, identical to its contribution to April-May precipitation. Thus, the monsoon moisture source region is dominated by contributions from the same general ocean area as that for April-May, and no major source shifts between ocean basins or ocean and continental sources are indicated.

The isotopic composition of the dominant ocean vapor source fluxes shows substantial differences during April-May and July-August (Fig. 5). The LMDZ4 model gives evaporation flux values of -4%~-

8‰ during April-May but about $1\%\sim3\%$ during July-August for this region. Estimated flux compositions for other vapor-contributing regions vary as well. Evapotranspiration δ^{18} O values are - $2\%\sim-5\%$ over southeast China and - $6\%\sim-7\%$ over Indochina during April-May, and decrease to - $8\%\sim-11\%$ over these regions in July-August (Fig. 5). To quantify the difference between seasons, we calculated the weighted (by boundary layer moisture source fractional contribution) mean evaporation δ^{18} O values (Table 1). Results show that the evaporation δ^{18} O value during April-May is 1.83% lower than during July-August, which is opposite to the seasonal precipitation δ^{18} O pattern for R_East (Fig. 1 and 2; Table 1). These results suggest that moisture source changes cannot explain the drop in R_East precipitation δ^{18} O values during summer monsoon onset.

4.3 Large-scale atmospheric controls

Precipitation δ^{18} O values can also respond to fractionation and mixing history as water vapor is transported from its source region to sites of precipitation. Using the previously identified moisture source regions, we explored the influence of atmospheric controls on R_East precipitation δ^{18} O values. For this purpose we defined a key region encompassing the major moisture uptake locations and transport paths and bordering the R_East focus area (Fig. 4).

Convection and moisture convergence intensity has previously been identified as a primary control on tropical precipitation and vapor isotope compositions (Kurita, 2013; Moore et al., 2014; Risi et al., 2008a; Worden et al., 2007) and these influences on water vapor can be felt in downstream sites (e.g., He et al., 2015; Risi et al., 2008b). Here we use CTP and CTT to measure this factor. Monthly precipitation δ^{18} O values from R_East are positively correlated with CTP over the key region (Fig. 6a), with correlation coefficients of 0.54 to 0.76 at the Changsha, Guilin, and Liuzhou monitoring sites (Table

S1). These correlations are much stronger than those previously reported at the same sites against local precipitation amount (Fig. 3). The weakest correlation with CTP is observed at Changsha and may be related to its northern location (see below). Similarly, the precipitation δ^{18} O also significantly correlates with CTT over the key moisture source region (Fig. 6b).

Precipitation δ^{18} O values decrease with intensified convection (reflected by lower CTP and CTT values) over the moisture source region, suggesting that isotopic effects of convection in this region may be propagated to the down-stream monitoring sites analyzed here. To understand this effect, we analyzed satellite-derived vertical profiles of specific humidity (q) and δD during April-May and July-August over the key moisture source region (Fig. S4). At near surface levels, vapor isotope ratios are strongly influenced by surface evaporation. This influence from surface evaporation produces higher vapor isotope ratios during July-August (Fig. S4 and Fig. 5). In contrast, the lower- to mid-troposphere is characterized by higher specific humidity and lower δD during July-August as compared with April-May (Fig. S4).

We used q- δD plots (for measurements over the key moisture source region) and compared the plots with theoretical Rayleigh distillation curves to assess the cause of isotopic depletion of source region lower-troposphere water vapor during the monsoon season (Fig. 7). This technique has been widely used to study processes controlling vapor isotope compositions (e.g., Brown et al., 2008; Galewsky et al., 2016; Worden et al., 2007), and leverages the different isotopic 'pathways' associated with airmass moistening and drying driven by different atmospheric processes. We calculated theoretical Rayleigh curves with initial δD equal to evaporation δD values derived from LMDZ outputs over the key moisture source region and starting from air parcels with saturation specific humidity at surface air temperature.

In addition, we calculated mixing curves to show the effect of mixing with surface evaporation. The dry end-member of the mixing curve has specific humidity of 0.5 g/kg and δD of -500‰, and the wet end-member shares the same specific humidity and δD with initial air parcels for the corresponding Rayleigh curve.

357

358

359

360

361

362

363

364

365

366

367

368

369

370

371

372

373

374

375

376

377

To show the link between vapor δD in the moisture source region and precipitation $\delta^{18}O$ at the study sites, we only plotted δD measurements at lower-troposphere (between 1000-750 hPa) where most moisture uptake occurs (the boundary layer criterion has been relaxed here as the analysis is not restricted to surface evaporation). Histograms of moisture uptake altitude show that moisture uptake mainly occurs in the lower-troposphere and ~95% of uptake happens below the 750 hPa level during both April-May and July-August (Fig. S5). We find that most April-May TES q-δD measurements are centered on the Rayleigh curve (Fig. 7a), consistent with dehydration of air containing ocean vapor-sourced moisture as the dominant driver of isotopic variability. During July-August, a larger number of TES measurements are shifted below the Rayleigh curve (Fig. 7b). Several processes may work to shift δD below the Rayleigh curve: unsaturated downdrafts (Risi et al., 2008a) or mesoscale downdrafts (Kurita, 2013; Kurita et al., 2011) bring D-depleted mid-troposphere vapor downward and mixing with lowertroposphere vapor; rain droplet re-evaporation (Worden et al., 2007) or vapor-droplet isotope exchange (Rozanski et al., 1993) also bring D-depleted vapor to the lower-troposphere. In addition, strong mixing with, or large contribution from, surface evaporation shifts δD above the Rayleigh curve (e.g., many measurements in Fig. 7a fall above the Rayleigh curve) (e.g., Noone, 2012; Worden et al., 2007). In contrast, strong convergence of more depleted surrounding vapor in deep convection systems isotopically depletes lower-troposphere vapor (Lee et al., 2007; Moore et al., 2014). Each of these

processes provides a potential link between deep convection and lower-troposphere vapor isotope ratios.

Thus the July-August TES data suggest the influence of convective intensity on lower-troposphere vapor isotope ratios in the source region, and potential for this convection signal to be propagated to and influence isotope values at downwind sites.

Seasonal variation in the strength of the monsoon trough and north-south migration of the ITCZ are the two major factors influencing convection intensity in the R_East key moisture source region (e.g., Wang, 2006). To further explore the relationship between precipitation δ^{18} O values and large-scale atmospheric circulation patterns we analyzed the relationship between precipitation δ^{18} O values and the mean latitudinal position of the ITCZ (Fig. 6c and Table S1). Our estimate of the position of the ITCZ is limited to the longitude band of the key moisture source region (100-135°E) and is based on midtroposphere ascending air motion, and thus also represents the center of the monsoon trough in the northern Hemisphere. The result shows that monthly precipitation δ^{18} O values at the three stations are strongly associated with the north-south movement of the ITCZ (Fig. 6c and Table S1): when the ITCZ is located further north, precipitation isotope values are lower, and vice versa. A one-degree northward advancement of the ITCZ corresponds to a ~0.3%~0.4% decrease in precipitation δ^{18} O values (Table S1).

The early-summer drop in δ^{18} O values occurs about one month later at Changsha than that at the other R_East stations (Fig. 8a). The one month lag may reflect a delay in the propagation of the ITCZ influence to the location of Changsha. Changsha is 3.5 degrees north of Guilin and Liuzhou, a value that is similar to the rate of northward movement of the ITCZ between May and June (3.1 degrees/month; Fig. 8b). Accounting for this one-month lag, seasonal δ^{18} O variation at Changsha is also synchronized

with the propagation of the ITCZ, and the weaker correlations between Changsha precipitation $\delta^{18}O$ values and convection intensity and ITCZ positon are improved substantially (Table S1).

4.4 A comparative study in south Asia

We test the generality of our findings across the AM region by conducting an equivalent set of analyses for R_STP (Fig. 9). Monthly total attributed moisture amounts for this region compare favorably against regional mean TRMM precipitation amounts (r = 0.95, p < 0.01; Fig. S6). Compared with R_East, better performance of the moisture attribution method in R_STP may be due to the larger precipitation variability in R_STP during April, May, July, and August (Fig. S2 and S6).

Results show that oceanic moisture from the Bay of Bengal is the dominant source for R_STP precipitation both during April-May and July-August (Fig. 9a and 9b). A small amount of moisture is derived from the east Arabian Sea during April-May (Fig. 9a) and from the west Arabian Sea during July-August (Fig. 9b). Similar to results for R_East, moisture uptake within the boundary layer dominates and has a similar spatial pattern to total moisture uptake (Fig. S7). The weighted (by boundary layer moisture source contribution) mean evaporation δ^{18} O value for R_STP sources is -5.93‰ in April-May and -5.89‰ in July-August (Table 1). In contrast, the difference in R_STP precipitation δ^{18} O values between these periods is over 4.60‰ based on observations at the three stations (Table 1). These results are consistent with those from R_East, showing that for both regions neither continental-oceanic moisture source shift nor changes in source vapor isotopic composition can explain the sharp drop in precipitation δ^{18} O values during summer monsoon onset.

Using the moisture source attribution we defined a key source region for R_STP and analyzed the relationship between key region monthly convection intensity and precipitation $\delta^{18}O$ values at three

stations in R_STP (Fig. 9c). Due to limitation in the temporal coverage of cloud data, we used vertical velocity at 500 hPa (ω) as an alternative metric of convection intensity. As frequency of cyclonic activity may be not reflected in monthly mean ω and post-monsoon ¹⁸O depletion is not the main focus of this study, we choose to exclude those months (October-December) during post-monsoon season in this section.

As was the case for R_East, we found robust correlations between R_STP monthly precipitation $\delta^{18}O$ values and convection intensity, with correlation coefficients equal to or higher than 0.80 (Fig. 9c). Precipitation $\delta^{18}O$ values decrease with intensified mid-troposphere upward air motion (more negative ω), and high precipitation $\delta^{18}O$ values are associated with shallow convection or weak water vapor convergence marked by descending motion in the mid-troposphere (Fig. 9c). TES q- δD measurements over the key moisture source region also show shifts of q- δD between April-May and July-August, consistent with the aforementioned deep convection effects on lower-troposphere vapor isotope compositions during July-August (Fig. S8). In addition, monthly precipitation $\delta^{18}O$ values are negatively correlated with the mean latitudinal position of ITCZ in the R_STP key region band of 75-95°E (Fig. 9a and 9d). These results, together with results from R_East, demonstrate that regional convection intensity, driven by large-scale atmospheric circulation, is a general control on precipitation $\delta^{18}O$ values in the AM region.

4.5 Paleoclimate implications

Despite persistent controversy regarding the climatic interpretation of paleo- δ^{18} O records from archives in the AM region, it has become consensual that these records are intimately related to and reflect past precipitation δ^{18} O variability (e.g., Cheng et al., 2016; Liu et al., 2015; Thompson et al.,

2000; Wang et al., 2001). Therefore, a clearer understanding of the empirically defined amount effect and controlling mechanisms in the AM region is needed to improve our reconstruction of past monsoon climate. Three major paradigms have been advanced to this end. The first relates precipitation or proxy δ^{18} O interpretation to local precipitation amount, for example due to a correlation between precipitation amount and rainout intensity (e.g., Liu et al., 2015; Tan et al., 2018; Thompson et al., 2000; Tian et al., 2003). Our results imply that precipitation δ^{18} O values do not respond directly to local precipitation amounts, but rather reflect large-scale dynamical forcing across the region. Moreover, the pattern documented here produces insignificant correlations between precipitation δ^{18} O values and local precipitation amounts in southeast China, where many speleothem records have been obtained, compromising even empirically-based paleo-precipitation reconstruction in this area. However, high precipitation rates during the pre-monsoon season in this region imply that past changes in precipitation seasonality (Cheng et al., 2016; Wang et al., 2001) could have significantly affected annual average δ^{18} O values, which may be reflected in paleo archives.

Second, although recent work on moisture sources has contributed to our understanding of transport paths as a driver of precipitation isotope ratios in some regions, and allowed reconstruction of past circulation changes, it appears that this model is not adequate to explain seasonal precipitation $\delta^{18}O$ change in the AM region.

Instead, we demonstrate that seasonal precipitation isotope variation in the AM region is linked to a third mechanism involving large-scale atmospheric controls on regional convection intensity. The timing of precipitation δ^{18} O value drop during late-spring to early-summer coincides with the timing of northward ITCZ/monsoon trough migration, with a lag, for example, between northern and southern

sites reflecting the progressive advance of the East Asian Summer Monsoon (Wang, 2006; Wang and LinHo, 2002). The earlier 18 O-depletion noted here for two southern sites in the R_East area can also be observed at other southern AM sites such as Hong Kong (Fig. 1g), Haikou (Fig. 1j), and Diliman (Fig. 1j), whereas slightly delayed 18 O-depletion is characteristic of many more northern sites, e.g., Wuhan (Fig. 1f) and Nanjing (Fig. 1h). These results suggest that interpretations of paleoclimate proxy data in terms of either local precipitation amounts or vapor transport may be questionable, but demonstrates new potential to use precipitation δ^{18} O values to spatially delineate the timing and extent of summer monsoon water cycling today and in the past.

4.6 Uncertainties and Limitations

Although this study provides support for a coherent mechanism for seasonal precipitation isotope variation across the AM region, we acknowledge that limitations to our analysis leave room for continued work on the topic. Our moisture source identification and attribution uses only a single precipitation level in order to limit computational time and cost. Although our results are consistent with a previous study using a more comprehensive multi-level analysis (Li et al., 2016), additional work to more accurately isolate the condensation level is warranted to fully resolve moisture sources for total precipitation. Another uncertainty in our study regards limitations to the evaporation flux isotope estimates derived from the LMDZ4 model, especially over the continent. The lack of a land-surface isotopic fractionation scheme in this model, a limitation common to most other General Circulation Models implementations thus far (Risi et al., 2012), limits our ability to assess how terrestrial hydrological processes might affect the isotopic composition of this flux. In particular, we would expect larger errors when the evaporation-transpiration ratio is large. However, given that our analysis

suggested that moisture sources to our focus areas were primarily oceanic regions, this uncertainty should have a limited impact on the study.

5 Conclusions

483

484

485

486

487

488

489

490

491

492

493

494

495

496

497

498

499

500

Our analysis of the spatial-seasonal structure of Asian Monsoon region precipitation $\delta^{18}O$ values shows that precipitation δ^{18} O exhibits consistent seasonal variation, with high values before the summer monsoon onset and low values during the summer monsoon season. This pattern is prevalent across the region, despite precipitation amount seasonality that shows more diverse regional characteristics. Moisture source identification and attribution analysis for two regions with contrasting seasonal precipitation patterns indicates that in both regions isotopically distinct precipitation in pre-monsoon and monsoon-mature seasons is derived from moisture sources with similar continental-oceanic ratios and estimated isotope ratios. This result suggests that moisture source changes cannot explain seasonal Asian Monsoon region precipitation isotope ratio variations. Instead, we show that differences in regional convection intensity before and after monsoon onset are uniformly associated with seasonal change in precipitation isotope ratios across the study area. Precipitation δ^{18} O variation is strongly synchronized with the seasonal monsoon circulation and the north-south migration of ITCZ. Although our analyses are focused on monthly data and the seasonal time scale, these results indicate that the extent and strength of monsoon circulation and the ITCZ in the past may be resolved from spatial-temporal analysis of paleo-precipitation δ^{18} O reconstructed from this region.

501

502

503

Acknowledgements

We thank the editors and two anonymous reviewers for their comments and suggestions. The IAEA

(GNIP database) and the Third Pole Environment Database provided part of the precipitation isotope data. The NASA Jet Propulsion Laboratory provided the TES satellite data. The NASA Goddard Institute for Space Studies provided the ISCCP D2 products. The NASA Goddard Space Flight Center provided the TRMM and GPCP data. The NOAA/OAR/ESRL PSD provided OLR data. The ECMWF Public Datasets web interface provided the ERA-Interim data. The NOAA Air Resources Laboratory (ARL) provided the HYSPLIT transport and dispersion model (http://ready.arl.noaa.gov/HYSPLIT.php). We thank the SWING2 group for providing the model isotope data. This research was supported by the National Natural Science Foundation of China (Grant Nos. 41771043, 41530748, & 41701080). Z. Cai was partially supported by the State Scholarship Fund of China Scholarship Council, and GJB was supported by US National Science Foundation grant EF-1241286.

514

515

504

505

506

507

508

509

510

511

512

513

References

- Aggarwal, P.K., Fröhlich, K., Kulkarni, K.M., Gourcy, L.L., 2004. Stable isotope evidence for moisture
- sources in the asian summer monsoon under present and past climate regimes. Geophys. Res. Lett.
- 518 31, L08203. doi:10.1029/2004GL019911.
- 519 Araguás-Araguás, L., Fröehlich, K., Rozanski, K., 1998. Stable isotope composition of precipitation
- over southeast Asia. J. Geophys. Res. 103, 28721-28742.
- Bowen, G.J., 2008. Spatial analysis of the intra-annual variation of precipitation isotope ratios and its
- 522 climatological corollaries. J. Geophys. Res. 113, D05113. doi:10.1029/2007jd009295.
- Bowen, G.J., West, J.B., Miller, C.C., Zhao, L., Zhang, T., 2017. IsoMAP: Isoscapes Modeling, Analysis
- and Prediction (version 1.0). The IsoMAP Project. http://isomap.org.

- Bowen, G.J., Wilkinson, B., 2002. Spatial distribution of δ^{18} O in meteoric precipitation. Geology 30,
- 526 315. doi:10.1130/0091-7613(2002)030<0315:sdooim>2.0.co;2.
- 527 Breitenbach, S.F.M., Adkins, J.F., Meyer, H., Marwan, N., Kumar, K.K., Haug, G.H., 2010. Strong
- influence of water vapor source dynamics on stable isotopes in precipitation observed in Southern
- Meghalaya, NE India. Earth Planet. Sci. Lett. 292, 212-220. doi:10.1016/j.epsl.2010.01.038.
- Brown, D., Worden, J., Noone, D., 2008. Comparison of atmospheric hydrology over convective
- continental regions using water vapor isotope measurements from space. J. Geophys. Res. 113.
- 532 doi:10.1029/2007jd009676.
- Cai, Z., Tian, L., 2016a. Atmospheric controls on seasonal and interannual variations in the precipitation
- isotope in the East Asian Monsoon region. J. Climate 29, 1339-1352. doi:10.1175/JCLI-D-15-
- 535 0363.1.
- 536 Cai, Z., Tian, L., 2016b. Processes Governing Water Vapor Isotope Composition in the Indo-Pacific
- Region: Convection and Water Vapor Transport. J. Climate 29, 8535-8546. doi:10.1175/jcli-d-16-
- 538 0297.1.
- Cai, Z., Tian, L., Bowen, G.J., 2017. ENSO variability reflected in precipitation oxygen isotopes across
- 540 the Asian Summer Monsoon region. Earth Planet. Sci. Lett. 475, 25-33.
- 541 doi:10.1016/j.epsl.2017.06.035.
- 542 Cheng, H., Edwards, R.L., Sinha, A., Spötl, C., Yi, L., Chen, S., Kelly, M., Kathayat, G., Wang, X., Li,
- X., Kong, X., Wang, Y., Ning, Y., Zhang, H., 2016. The Asian monsoon over the past 640,000 years
- and ice age terminations. Nature 534, 640-646. doi:10.1038/nature18591.
- Dansgaard, W., 1964. Stable isotopes in precipitation. Tellus 16, 436-468. doi:10.1111/j.2153-

- 546 3490.1964.tb00181.x.
- Dayem, K.E., Molnar, P., Battisti, D.S., Roe, G.H., 2010. Lessons learned from oxygen isotopes in
- modern precipitation applied to interpretation of speleothem records of paleoclimate from eastern
- Asia. Earth Planet. Sci. Lett. 295, 219-230. doi:10.1016/j.epsl.2010.04.003.
- Dee, D.P., Uppala, S.M., Simmons, A.J., Berrisford, P., Poli, P., Kobayashi, S., Andrae, U., Balmaseda,
- M.A., Balsamo, G., Bauer, P., Bechtold, P., Beljaars, A.C.M., van de Berg, L., Bidlot, J., Bormann,
- N., Delsol, C., Dragani, R., Fuentes, M., Geer, A.J., Haimberger, L., Healy, S.B., Hersbach, H.,
- Hólm, E.V., Isaksen, L., Kållberg, P., Köhler, M., Matricardi, M., McNally, A.P., Monge-Sanz, B.M.,
- Morcrette, J.J., Park, B.K., Peubey, C., de Rosnay, P., Tavolato, C., Thépaut, J.N., Vitart, F., 2011.
- The ERA-Interim reanalysis: configuration and performance of the data assimilation system. Q. J.
- 856 Roy. Meteorol. Soc. 137, 553-597. doi:10.1002/qj.828.
- 557 Galewsky, J., Steen-Larsen, H.C., Field, R.D., Worden, J., Risi, C., Schneider, M., 2016. Stable isotopes
- in atmospheric water vapor and applications to the hydrologic cycle. Rev. Geophys., n/a-n/a.
- 559 doi:10.1002/2015RG000512.
- He, Y., Risi, C., Gao, J., Masson-Delmotte, V., Yao, T., Lai, C.-T., Ding, Y., Worden, J., Frankenberg, C.,
- 561 Chepfer, H., Cesana, G., 2015. Impact of atmospheric convection on south Tibet summer
- precipitation isotopologue composition using a combination of in situ measurements, satellite data
- and atmospheric general circulation modeling. J. Geophys. Res. 120, 3852-3871.
- 564 doi:10.1002/2014JD022180.
- Huffman, G.J., Bolvin, D.T., Nelkin, E.J., Wolff, D.B., Adler, R.F., Gu, G., Hong, Y., Bowman, K.P.,
- Stocker, E.F., 2007. The TRMM Multisatellite Precipitation Analysis (TMPA): Quasi-Global,

- Multiyear, Combined-Sensor Precipitation Estimates at Fine Scales. J. Hydrometeorol. 8, 38-55.
- 568 doi:10.1175/jhm560.1.
- Kurita, N., 2013. Water isotopic variability in response to mesoscale convective system over the tropical
- ocean. J. Geophys. Res. 118, 10,376-310,390. doi:10.1002/jgrd.50754.
- Kurita, N., Noone, D., Risi, C., Schmidt, G.A., Yamada, H., Yoneyama, K., 2011. Intraseasonal isotopic
- variation associated with the Madden-Julian Oscillation. J. Geophys. Res. 116, D24101.
- 573 doi:10.1029/2010JD015209.
- Lee, J.-E., Fung, I., DePaolo, D.J., Henning, C.C., 2007. Analysis of the global distribution of water
- isotopes using the NCAR atmospheric general circulation model. J. Geophys. Res. 112, D16306.
- 576 doi:10.1029/2006JD007657.
- Lekshmy, P.R., Midhun, M., Ramesh, R., 2015. Spatial variation of amount effect over peninsular India
- 578 and Sri Lanka: Role of seasonality. Geophys. Res. Lett. 42, 5500-5507. doi:10.1002/2015gl064517.
- 579 Li, L.T., Dolman, A.J., Xu, Z.X., 2016. Atmospheric moisture sources, paths, and the quantitative
- importance to the Eastern Asian Monsoon region. J. Hydrometeorol. 17, 637-649.
- 581 doi:10.1175/JHM-D-15-0082.1.
- Liu, J., Chen, J., Zhang, X., Li, Y., Rao, Z., Chen, F., 2015. Holocene East Asian summer monsoon
- records in northern China and their inconsistency with Chinese stalagmite δ^{18} O records. Earth-
- Science Reviews 148, 194-208. doi:10.1016/j.earscirev.2015.06.004.
- Moore, M., Kuang, Z., Blossey, P.N., 2014. A moisture budget perspective of the amount effect. Geophys.
- 586 Res. Lett. 41, 1329-1335. doi:10.1002/2013GL058302.
- Noone, D., 2012. Pairing Measurements of the Water Vapor Isotope Ratio with Humidity to Deduce

- Atmospheric Moistening and Dehydration in the Tropical Midtroposphere. J. Climate 25, 4476-
- 589 4494. doi:10.1175/jcli-d-11-00582.1.
- Peng, T.-R., Wang, C.-H., Huang, C.-C., Fei, L.-Y., Chen, C.-T.A., Hwong, J.-L., 2010. Stable isotopic
- characteristic of Taiwan's precipitation: A case study of western Pacific monsoon region. Earth
- 592 Planet. Sci. Lett. 289, 357-366. doi:10.1016/j.epsl.2009.11.024.
- Risi, C., Bony, S., Vimeux, F., 2008a. Influence of convective processes on the isotopic composition
- $(\delta^{18}O \text{ and } \delta D)$ of precipitation and water vapor in the tropics: 2. Physical interpretation of the
- amount effect. J. Geophys. Res. 113, D19306. doi:10.1029/2008JD009943.
- Risi, C., Bony, S., Vimeux, F., Descroix, L., Ibrahim, B., Lebreton, E., Mamadou, I., Sultan, B., 2008b.
- What controls the isotopic composition of the African monsoon precipitation? Insights from event-
- based precipitation collected during the 2006 AMMA field campaign. Geophys. Res. Lett. 35,
- 599 L24808. doi:10.1029/2008GL035920.
- Risi, C., Bony, S., Vimeux, F., Jouzel, J., 2010. Water-stable isotopes in the LMDZ4 general circulation
- model: Model evaluation for present-day and past climates and applications to climatic
- interpretations of tropical isotopic records. J. Geophys. Res. 115. doi:10.1029/2009jd013255.
- Risi, C., Noone, D., Worden, J., Frankenberg, C., Stiller, G., Kiefer, M., Funke, B., Walker, K., Bernath,
- P., Schneider, M., Wunch, D., Sherlock, V., Deutscher, N., Griffith, D., Wennberg, P.O., Strong, K.,
- Smale, D., Mahieu, E., Barthlott, S., Hase, F., García, O., Notholt, J., Warneke, T., Toon, G., Sayres,
- D., Bony, S., Lee, J., Brown, D., Uemura, R., Sturm, C., 2012. Process-evaluation of tropospheric
- humidity simulated by general circulation models using water vapor isotopologues: 1. Comparison
- between models and observations. J. Geophys. Res. 117, D05303. doi:10.1029/2011jd016621.

- Rossow, W.B., Schiffer, R.A., 1999. Advances in understanding clouds from ISCCP. Bull. Am. Meteorol.
- 610 Soc. 80, 2261-2287. doi:10.1175/1520-0477(1999)080<2261:Aiucfi>2.0.Co;2.
- Rozanski, K., Araguás-Araguás, L., Gonfiantini, R., 1993. Isotopic patterns in modern global
- precipitation, Climate Change in Continental Isotopic Records. AGU, Washington, DC, pp. 1-36.
- doi:10.1029/GM078p0001.
- 614 Sodemann, H., Schwierz, C., Wernli, H., 2008. Interannual variability of Greenland winter precipitation
- sources: Lagrangian moisture diagnostic and North Atlantic Oscillation influence. J. Geophys. Res.
- 616 113, n/a-n/a. doi:10.1029/2007JD008503.
- 617 Stein, A.F., Draxler, R.R., Rolph, G.D., Stunder, B.J.B., Cohen, M.D., Ngan, F., 2015. NOAA's
- HYSPLIT atmospheric transport and dispersion modeling system. Bull. Am. Meteorol. Soc. 96,
- 619 2059-2077. doi:10.1175/BAMS-D-14-00110.1.
- Tan, L., Cai, Y., Cheng, H., Edwards, L.R., Gao, Y., Xu, H., Zhang, H., An, Z., 2018. Centennial- to
- decadal-scale monsoon precipitation variations in the upper Hanjiang River region, China over the
- past 6650 years. Earth Planet. Sci. Lett. 482, 580-590. doi:10.1016/j.epsl.2017.11.044.
- Tang, Y., Pang, H., Zhang, W., Li, Y., Wu, S., Hou, S., 2015. Effects of changes in moisture source and
- the upstream rainout on stable isotopes in precipitation a case study in Nanjing, eastern China.
- 625 Hydrol. Earth Syst. Sci. 19, 4293-4306. doi:10.5194/hess-19-4293-2015.
- Thompson, L.G., Yao, T., E.Mosley-Thompson, Davis, M.E., Henderson, K.A., Lin, P.-N., 2000. A High-
- Resolution Millennial Record of the South Asian Monsoon from Himalayan Ice Cores. Science 289,
- 628 1916-1919. doi:10.1126/science.289.5486.1916.
- Tian, L., Yao, T., Schuster, P.F., White, J.W.C., Ichiyanagi, K., Pendall, E., Pu, J., Yu, W., 2003. Oxygen-

- 18 concentrations in recent precipitation and ice cores on the Tibetan Plateau. J. Geophys. Res. 108.
- 631 doi:10.1029/2002jd002173.
- Vimeux, F., Gallaire, R., Bony, S., Hoffmann, G., Chiang, J.C.H., 2005. What are the climate controls
- on δD in precipitation in the Zongo Valley (Bolivia)? Implications for the Illimani ice core
- interpretation. Earth Planet. Sci. Lett. 240, 205-220. doi:10.1016/j.epsl.2005.09.031.
- Wang, B., 2006. The Asian monsoon. Springer-Verlag Berlin Heidelberg, New York. doi:10.1007/3-540-
- 636 37722-0.
- Wang, B., LinHo, 2002. Rainy season of the Asian–Pacific summer monsoon. J. Climate 15, 386-398.
- doi:10.1175/1520-0442(2002)015<0386:RSOTAP>2.0.CO;2.
- 639 Wang, Y.J., Cheng, H., Edwards, R.L., An, Z.S., Wu, J.Y., Shen, C.C., Dorale, J.A., 2001. A high-
- resolution absolute-dated Late Pleistocene monsoon record from Hulu Cave, China. Science 294,
- 641 2345-2348. doi:10.1126/science.1064618.
- Worden, J., Bowman, K., Noone, D., Beer, R., Clough, S., Eldering, A., Fisher, B., Goldman, A., Gunson,
- M., Herman, R., Kulawik, S.S., Lampel, M., Luo, M., Osterman, G., Rinsland, C., Rodgers, C.,
- Sander, S., Shephard, M., Worden, H., 2006. Tropospheric Emission Spectrometer observations of
- the tropospheric HDO/H₂O ratio: Estimation approach and characterization. J. Geophys. Res. 111,
- 646 D16309. doi:10.1029/2005JD006606.
- Worden, J., Kulawik, S., Frankenberg, C., Payne, V., Bowman, K., Cady-Peirara, K., Wecht, K., Lee,
- J.E., Noone, D., 2012. Profiles of CH₄, HDO, H₂O, and N₂O with improved lower tropospheric
- vertical resolution from Aura TES radiances. Atmos. Meas. Tech. 5, 397-411. doi:10.5194/amt-5-
- 650 397-2012.

- Worden, J., Noone, D., Bowman, K., 2007. Importance of rain evaporation and continental convection
- in the tropical water cycle. Nature 445, 528-532. doi:10.1038/nature05508.
- Xie, L., Wei, G., Deng, W., Zhao, X., 2011. Daily δ^{18} O and δD of precipitations from 2007 to 2009 in
- Guangzhou, South China: Implications for changes of moisture sources. J. Hydrol. 400, 477-489.
- doi:10.1016/j.jhydrol.2011.02.002.
- Ku, C., Zheng, H., Nakatsuka, T., Sano, M., Li, Z., Ge, J., 2015. Inter- and intra-annual tree-ring cellulose
- oxygen isotope variability in response to precipitation in Southeast China. Trees, 1-10.
- doi:10.1007/s00468-015-1320-2.
- Yang, X., Davis, M.E., Acharya, S., Yao, T., 2017. Asian monsoon variations revealed from stable
- isotopes in precipitation. Clim. Dyn. doi:10.1007/s00382-017-4011-4.
- Yao, T., Ding, L., Pu, J., Ueda, Y., Ohata, T., Liu, J., Yang, Z., 1991. δ¹⁸O characteristics of snow at the
- Tanggula Mountains, on the Tibetan Plateau, and their relationship with moisture sources. Chin.
- 663 Sci. Bull. 20, 1570-1573. (in Chinese).
- Yao, T., Masson-Delmotte, V., Gao, J., Yu, W., Yang, X., Risi, C., Sturm, C., Werner, M., Zhao, H., He,
- Y., Ren, W., Tian, L., Shi, C., Hou, S., 2013. A review of climatic controls on δ^{18} O in precipitation
- over the Tibetan Plateau: Observations and simulations. Rev. Geophys., 2012RG000427.
- doi:10.1002/rog.20023.

Table 1. A comparison of weighted mean $\delta^{18}O$ of moisture source for R_East with precipitation $\delta^{18}O$ observed at Changsha (CS), Guilin (GL), and Liuzhou (LZ) for the two seasons: April-May (am), July-August (ja), and the difference between the two seasons (am-ja); and a comparison of weighted mean $\delta^{18}O$ of moisture source for R_STP with precipitation $\delta^{18}O$ observed at Dhaka (DK), Sylhet (SY), and Barisal (BA)

	R_East δ ¹⁸ O / ‰				R_STP δ ¹⁸ O / ‰			
	Source	CS	GL	LZ	Source	DK	SY	BA
am	-5.60	-2.63	-4.89	-4.79	-5.93	-1.46	-1.93	-2.84
ja	-3.77	-8.53	-8.57	-8.46	-5.89	-6.86	-7.25	-7.48
am-ja	-1.42	5.90	3.68	3.68	-0.04	5.40	5.32	4.64

- Figure captions:
- Fig. 1 Normalized long-term mean monthly precipitation amount (left column) and the corresponding
- precipitation δ^{18} O (right column) from stations clustered into groups 1 (a and f), 2 (b and g), 3 (c and h),
- 4 (d and i), and 5 (e and j). Shadings in the left column highlight peak precipitation season. Shadings in
- the right column highlight peak δ^{18} O values before summer monsoon onset and low values during
- monsoon season.
- 683 Fig. 2 Spatial distribution of the seasonal index SI derived from TRMM precipitation (a), IsoMAP
- processed CRU precipitation (b), and IsoMAP precipitation δ^{18} O (c); as well as spatial distribution of
- the correlation coefficient between IsoMAP precipitation δ^{18} O and precipitation amount (d, only values
- significant at p = 0.1 level are shown). The distribution of the five precipitation seasonality groups is
- plotted in (a). Values from station observations are also plotted in (b-d) (shading in circles). The
- rectangles in (a) shows the location of R East and R STP. Black lines denote the topography at 3000 m
- above sea level, indicating the southern boundary of the Tibetan Plateau.
- Fig. 3 Upper panel: relationships between monthly precipitation δ^{18} O and local precipitation amount for
- 691 Changsha (a), Guilin (b), and Liuzhou (c); lower panel: relationships between mean monthly GPCP
- precipitation amount over the region R East and precipitation δ^{18} O from Changsha (d), Guilin (e), and
- 693 Liuzhou (f).
- 694 Fig. 4 (a) and (b): spatial distribution of mean fractional moisture contribution (combined contribution
- from boundary layer and free troposphere) to precipitation in R East during April-May (a) and July-
- August (b) from 2000-2009. (c) and (d): the same as (a) and (b) but for boundary layer contribution only.
- Rectangles show the location of R East and stars show the location of back trajectory starting points.

- Dashed polygons show the identified key moisture source region for precipitation in R_East (see text for definition). Blue lines denote the topography at 3000 m above sea level, indicating the delineation of the Tibetan Plateau.
- Fig. 5 Spatial distribution of mean evaporation (and evapotranspiration over land) flux δ¹⁸O for April May (a) and July-August (b) from 2000-2009. Dash polygons indicate the key moisture source region
 for R_East and R_STP. Blue lines denote the topography at 3000 m above sea level, indicating the
 delineation of the Tibetan Plateau.
- Fig. 6 Relationships between monthly precipitation δ^{18} O (at Changsha, Guilin, and Liuzhou) and mean monthly cloud-top pressure (a) and cloud-top temperature (b) over the key moisture source region for

R East; (c): the same as (a), but between precipitation δ^{18} O and mean latitudinal ITCZ position.

707

717

718

708 Fig. 7 TES δD and specific humidity (q) measurements over the key moisture source region for R East 709 precipitation during April-May (a) and July-August (b) from 2006-2010 at lower-troposphere levels 710 (1000-750 hPa). Each point represents one measurement. Rayleigh curves (solid blue curves) were 711 calculated with initial δD equal to the mean value derived from LMDZ for source region evaporation 712 during those months (-34% in (a) and -22% in (b)) and initial specific humidity equal to saturation at 713 surface air temperature (298 K (a) and 302 K (b)). Mixing lines (solid purple curves) were calculated 714 using a dry end-member with q = 0.5 g/kg and $\delta D = -500\%$ and initial air parcels for the corresponding 715 Rayleigh curve as a wet end-member. Green contours show kernel density of TES q-δD measurements. Fig. 8 Long-term mean monthly precipitation δ^{18} O from Changsha, Guilin, Liuzhou, and R East average 716

in IsoMAP modeling (a); and long-term mean monthly R East key source region cloud-top temperature,

NOAA interpolated outgoing longwave radiation (OLR), and the mean latitudinal ITCZ position (b).

Error bars are standard deviations showing the interannual variability at each month (except for the IsoMAP modeling, which shows the standard deviations in the model predictions). Note that annual mean OLR value (240 W m $^{-2}$) has been subtracted from monthly values, and the y axis for ITCZ position is inversely plotted to improve readability.

Fig. 9 (a) and (b): spatial distribution of mean fractional moisture contribution to precipitation in R_STP during April-May (a) and July-August (b) from 2000-2009. Rectangles show the location of R_STP and stars show the location of back trajectory starting points. Location of Dhaka, Sylhet, and Barisal is shown as red crosses. Dashed polygons show the identified key moisture source region for precipitation in R_STP (see text for definition). Blue lines denote the topography at 3000 m above sea level, indicating the southern boundary of the Tibetan Plateau. (c) and (d): relationships between monthly precipitation δ^{18} O (at Dhaka, Sylhet, and Barisal) and mean monthly vertical velocity at 500 hPa (ω) over the key moisture source region for R_STP (c); and relationships between monthly precipitation δ^{18} O and mean latitudinal ITCZ position (d).

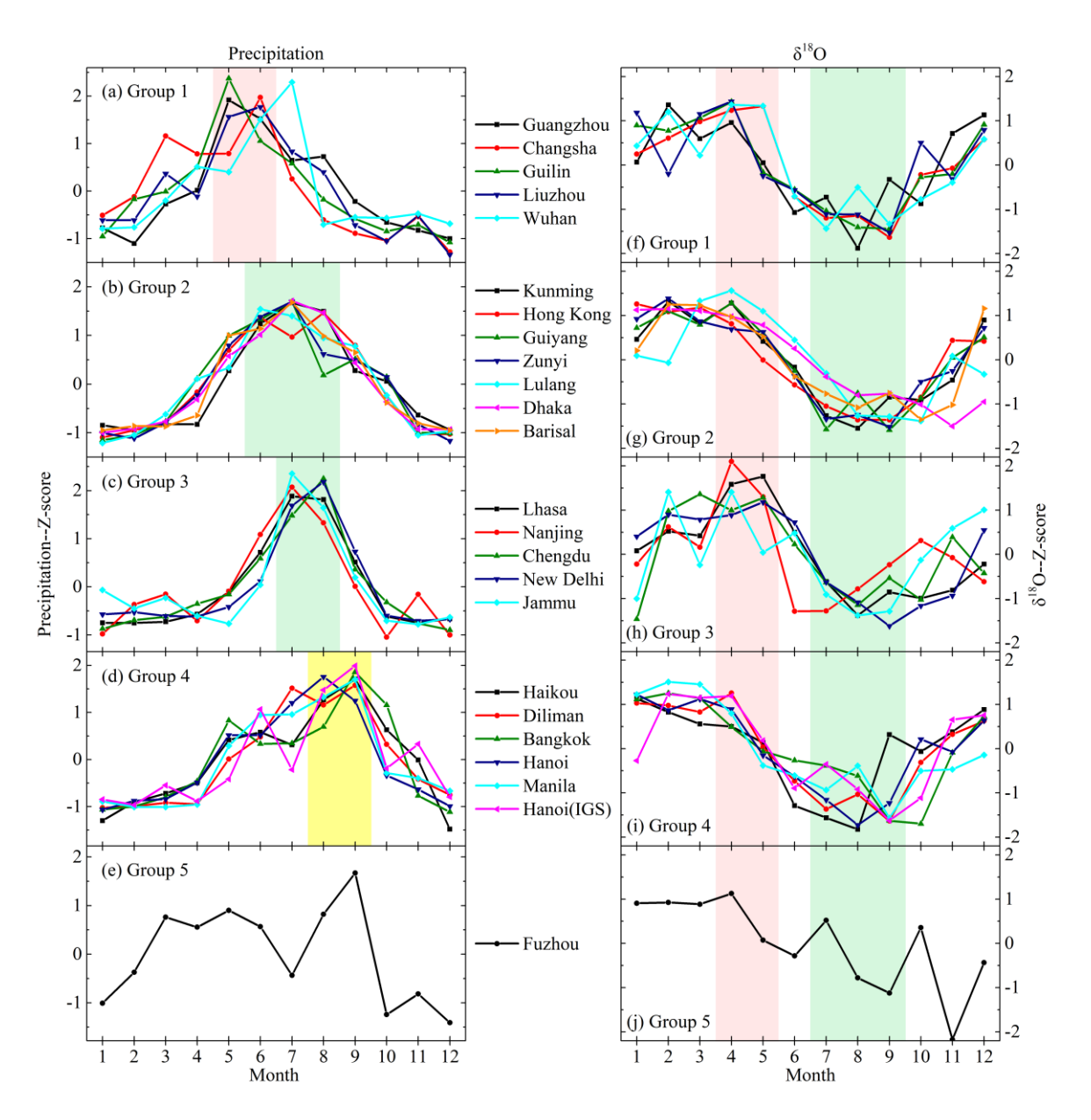


Fig. 1 Normalized long-term mean monthly precipitation amount (left column) and the corresponding precipitation $\delta^{18}O$ (right column) from stations clustered into groups 1 (a and f), 2 (b and g), 3 (c and h), 4 (d and i), and 5 (e and j). Shadings in the left column highlight peak precipitation season. Shadings in the right column highlight peak $\delta^{18}O$ values before summer monsoon onset and low values during monsoon season.

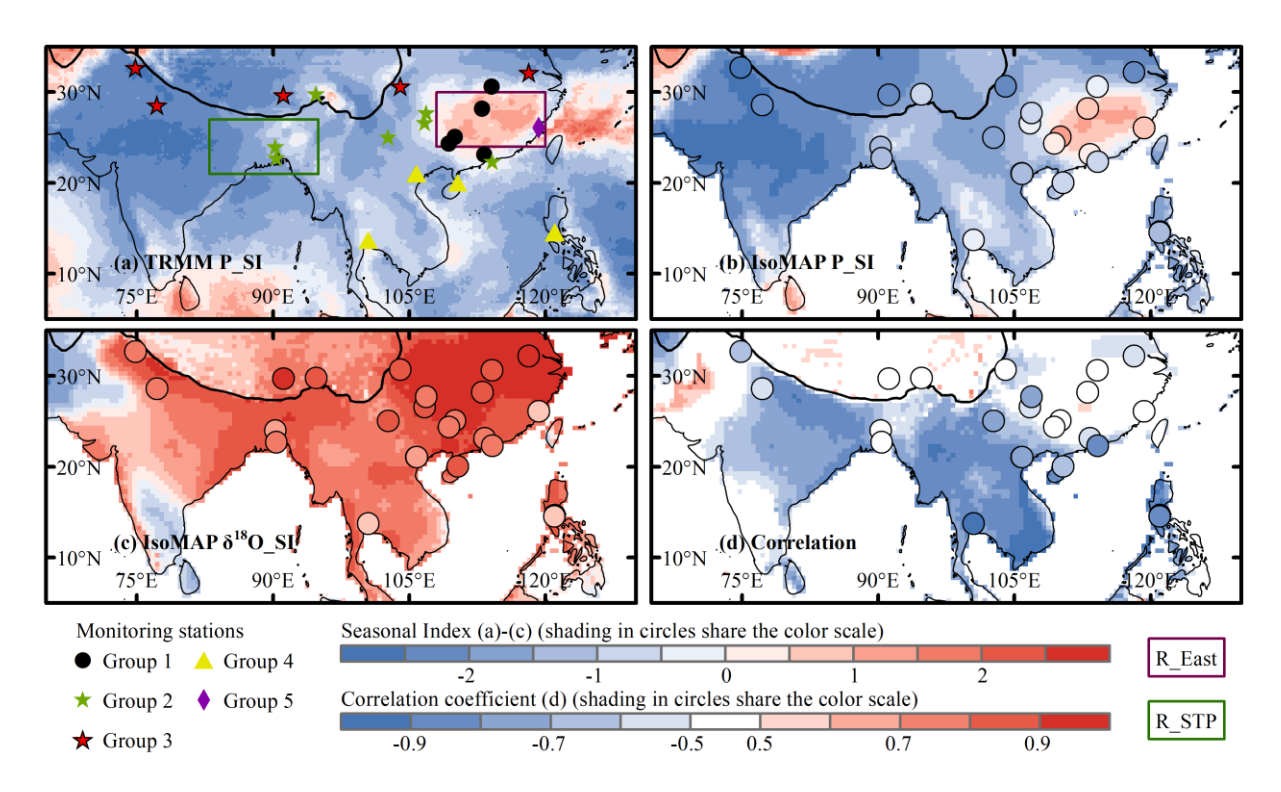


Fig. 2 Spatial distribution of the seasonal index SI derived from TRMM precipitation (a), IsoMAP processed CRU precipitation (b), and IsoMAP precipitation $\delta^{18}O$ (c); as well as spatial distribution of the correlation coefficient between IsoMAP precipitation $\delta^{18}O$ and precipitation amount (d, only values significant at p = 0.1 level are shown). The distribution of the five precipitation seasonality groups is plotted in (a). Values from station observations are also plotted in (b-d) (shading in circles). The rectangles in (a) shows the location of R_East and R_STP. Black lines denote the topography at 3000 m above sea level, indicating the southern boundary of the Tibetan Plateau.

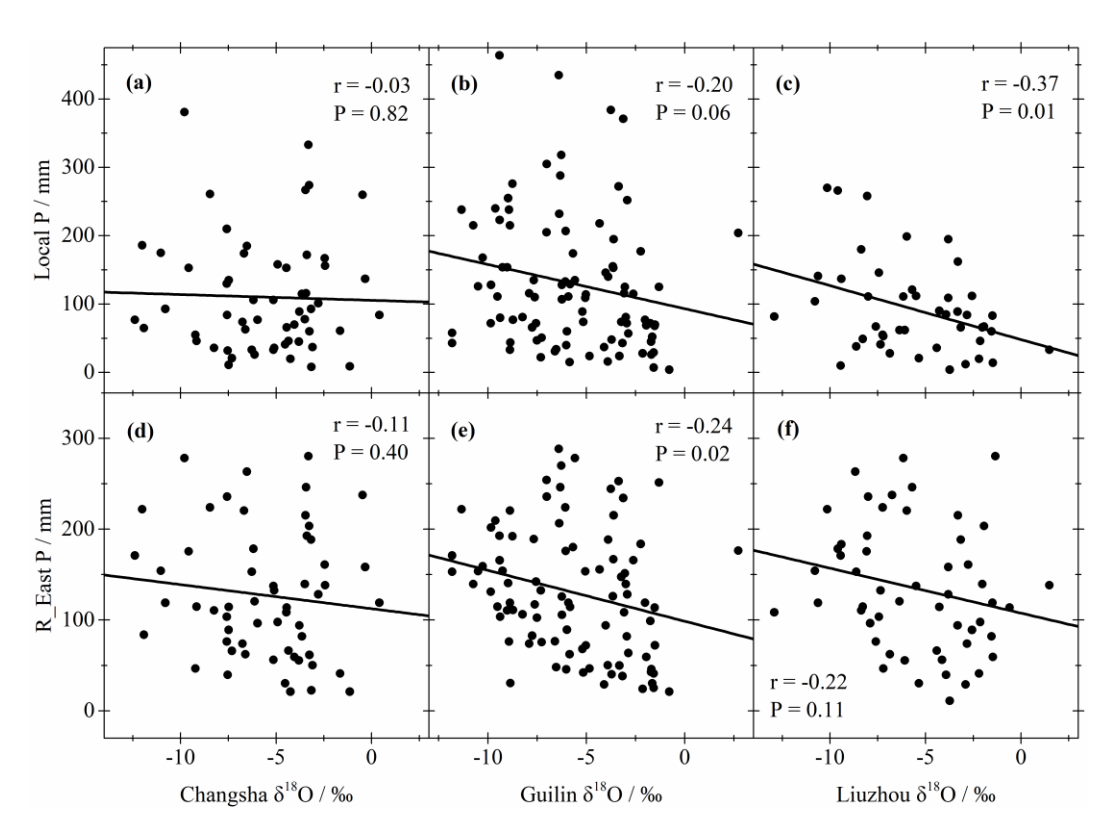


Fig. 3 Upper panel: relationships between monthly precipitation $\delta^{18}O$ and local precipitation amount for Changsha (a), Guilin (b), and Liuzhou (c); lower panel: relationships between mean monthly GPCP precipitation amount over the region R_East and precipitation $\delta^{18}O$ from Changsha (d), Guilin (e), and Liuzhou (f).

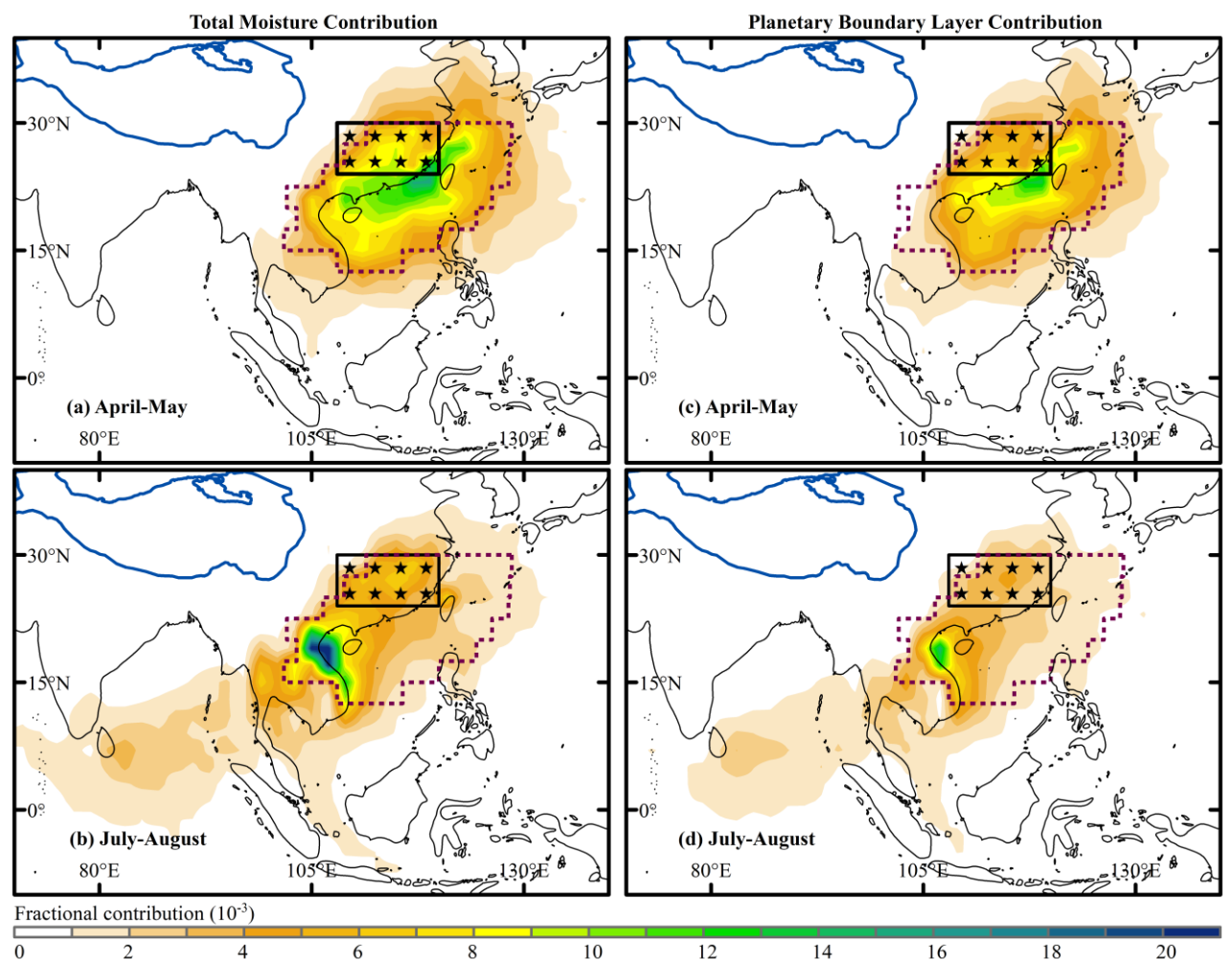


Fig. 4 (a) and (b): spatial distribution of mean fractional moisture contribution (combined contribution from boundary layer and free troposphere) to precipitation in R_East during April-May (a) and July-August (b) from 2000-2009. (c) and (d): the same as (a) and (b) but for boundary layer contribution only. Rectangles show the location of R_East and stars show the location of back trajectory starting points. Dashed polygons show the identified key moisture source region for precipitation in R_East (see text for definition). Blue lines denote the topography at 3000 m above sea level, indicating the delineation of the Tibetan Plateau.

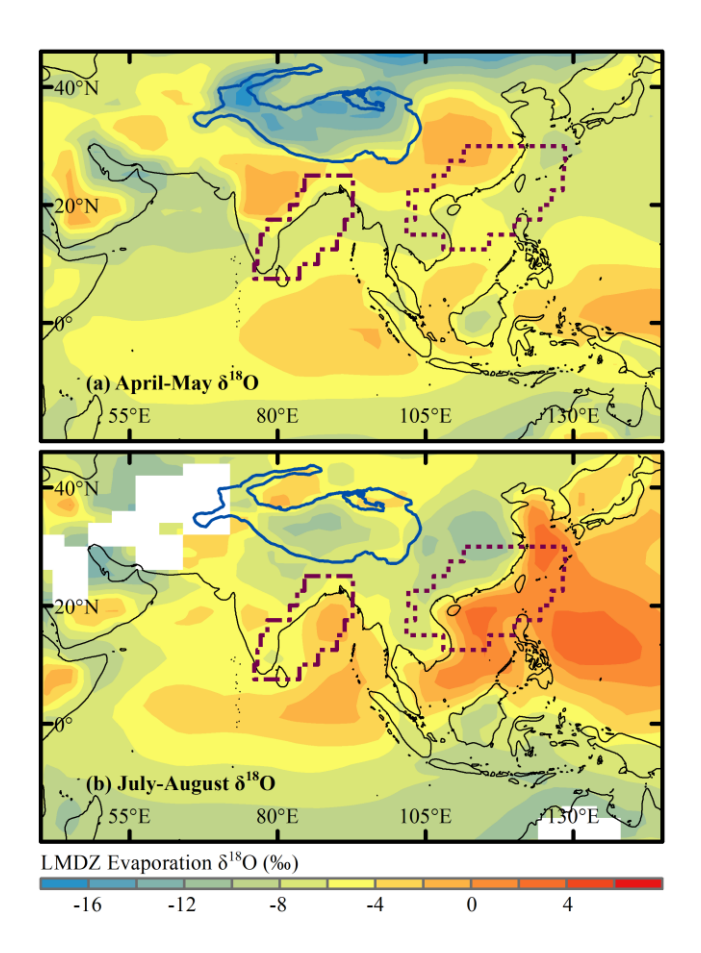


Fig. 5 Spatial distribution of mean evaporation (and evapotranspiration over land) flux $\delta^{18}O$ for April-May (a) and July-August (b) from 2000-2009. Dash polygons indicate the key moisture source region for R_East and R_STP. Blue lines denote the topography at 3000 m above sea level, indicating the delineation of the Tibetan Plateau.

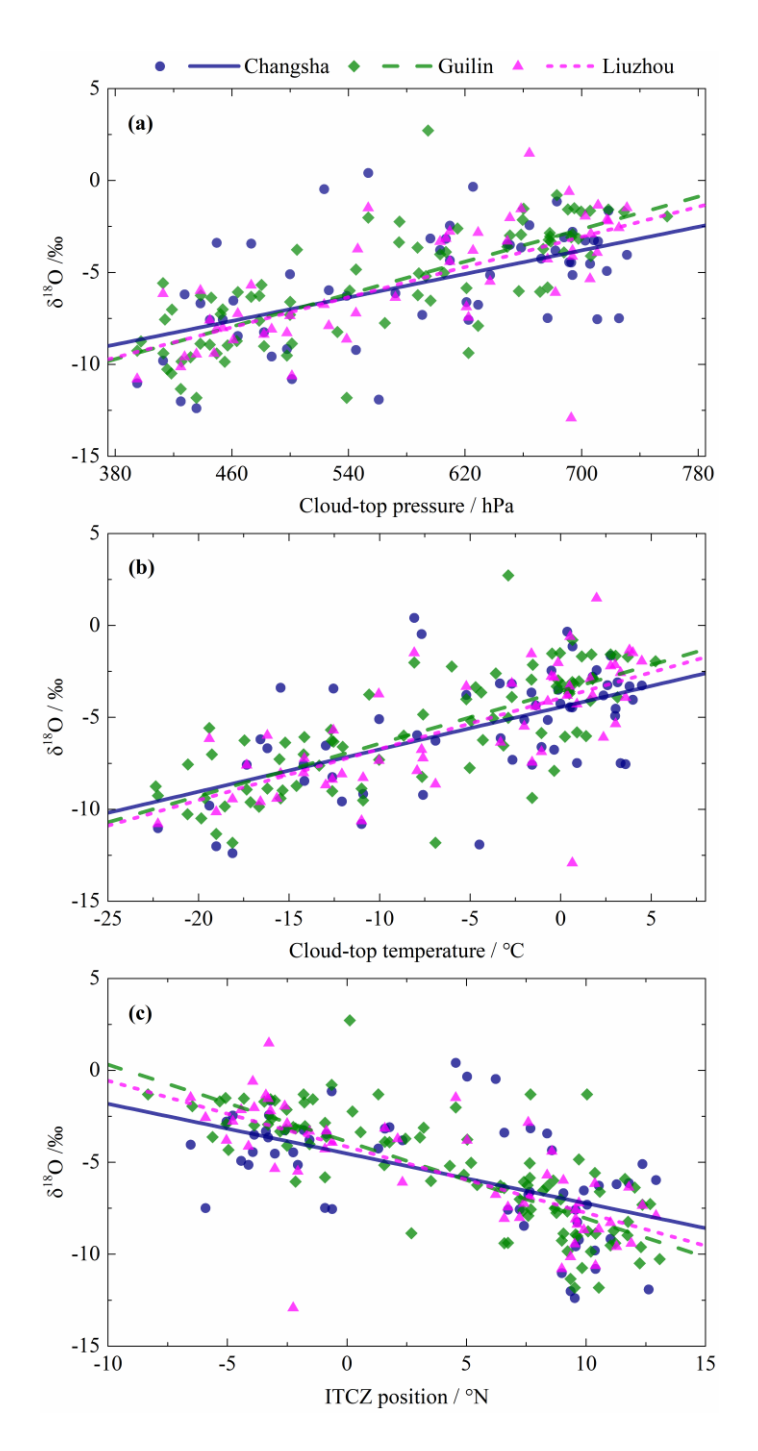


Fig. 6 Relationships between monthly precipitation $\delta^{18}O$ (at Changsha, Guilin, and Liuzhou) and mean monthly cloud-top pressure (a) and cloud-top temperature (b) over the key moisture source region for R_East; (c): the same as (a), but between precipitation $\delta^{18}O$ and mean latitudinal ITCZ position.

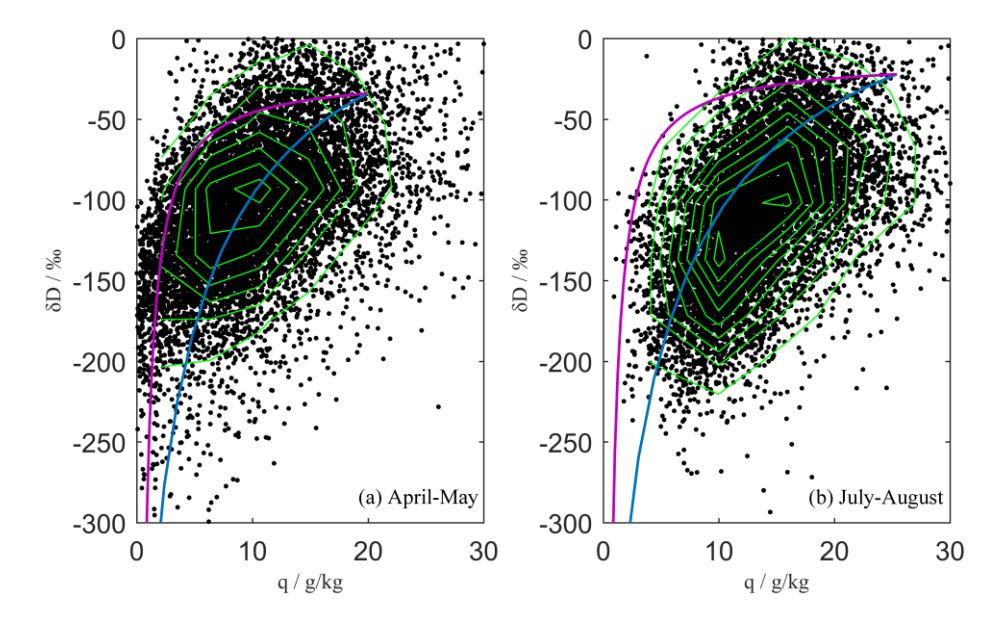


Fig. 7 TES δD and specific humidity (q) measurements over the key moisture source region for R_East precipitation during April-May (a) and July-August (b) from 2006-2010 at lower-troposphere levels (1000-750 hPa). Each point represents one measurement. Rayleigh curves (solid blue curves) were calculated with initial δD equal to the mean value derived from LMDZ for source region evaporation during those months (-34% in (a) and -22% in (b)) and initial specific humidity equal to saturation at surface air temperature (298 K (a) and 302 K (b)). Mixing lines (solid purple curves) were calculated using a dry end-member with q = 0.5 g/kg and $\delta D = -500\%$ and initial air parcels for the corresponding Rayleigh curve as a wet end-member. Green contours show kernel density of TES q- δD measurements.

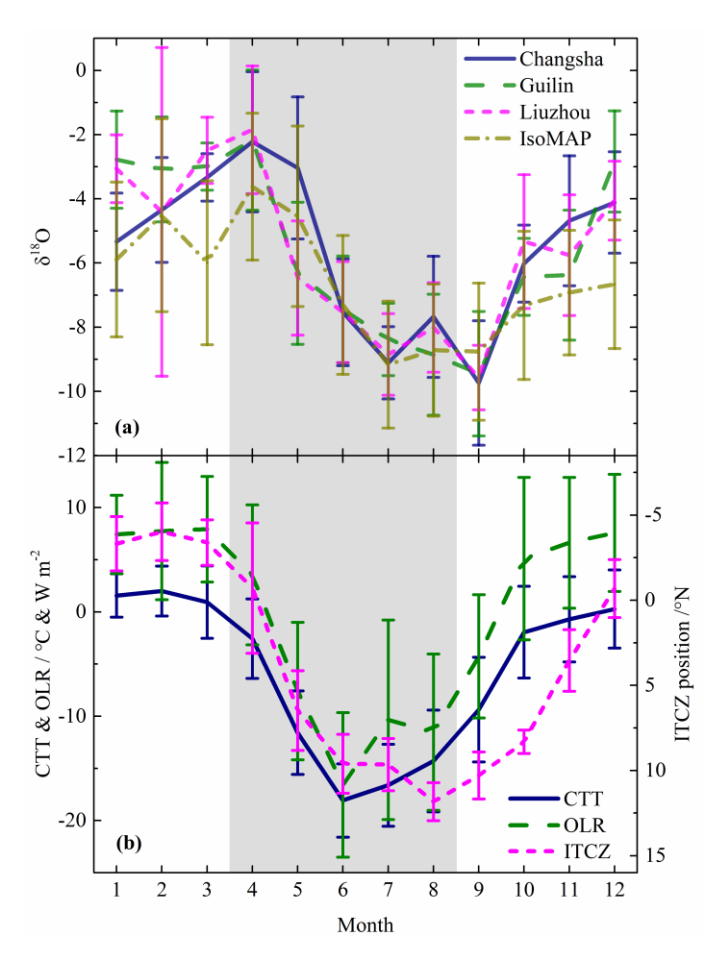


Fig. 8 Long-term mean monthly precipitation $\delta^{18}O$ from Changsha, Guilin, Liuzhou, and R_East average in IsoMAP modeling (a); and long-term mean monthly R_East key source region cloud-top temperature, NOAA interpolated outgoing longwave radiation (OLR), and the mean latitudinal ITCZ position (b). Error bars are standard deviations showing the interannual variability at each month (except for the IsoMAP modeling, which shows the standard deviations in the model predictions). Note that annual mean OLR value (240 W m⁻²) has been subtracted from monthly values, and the y axis for ITCZ position is inversely plotted to improve readability.

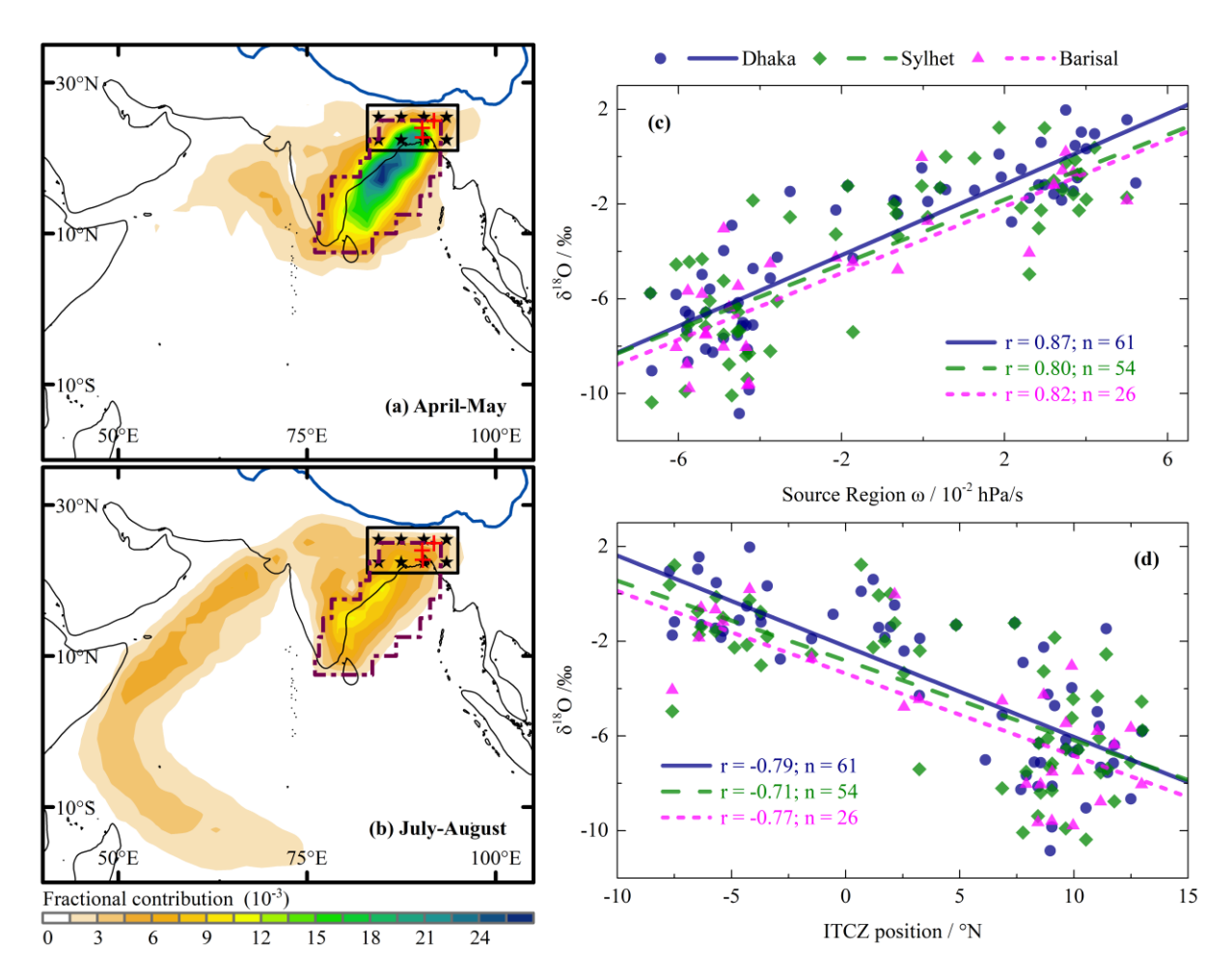


Fig. 9 (a) and (b): spatial distribution of mean fractional moisture contribution to precipitation in R_STP during April-May (a) and July-August (b) from 2000-2009. Rectangles show the location of R_STP and stars show the location of back trajectory starting points. Location of Dhaka, Sylhet, and Barisal is shown as red crosses. Dashed polygons show the identified key moisture source region for precipitation in R_STP (see text for definition). Blue lines denote the topography at 3000 m above sea level, indicating the southern boundary of the Tibetan Plateau. (c) and (d): relationships between monthly precipitation δ^{18} O (at Dhaka, Sylhet, and Barisal) and mean monthly vertical velocity at 500 hPa (ω) over the key moisture source region for R_STP (c); and relationships between monthly precipitation δ^{18} O and mean latitudinal ITCZ position (d).